Experimental investigation on a high head model Francis turbine during load rejection

Experimental investigation on a high head model Francis turbine during load rejection

R Goyal[1, 3], C Bergan[2], M J Cervantes[2, 3], B K Gandhi[1] and O G Dahlhaug[2]

[1] Indian Institute of Technology Roorkee, Roorkee, 247667 Roorkee, India
[2] Waterpower Laboratory, Norwegian University of Science and Technology, Alfred Getz vei 4, 7034 Trondheim, Norway
[3] Department of Eng. Sci. and Math, Luleå University of Technology, 97187 Luleå, Sweden

E-mail: goel.rahul87@gmail.com

Abstract. Francis-99 is a set of workshop aiming to determine the state of the art of high head model Francis turbine simulations (flow and structure) under steady and transient operating conditions as well as to promote their development and knowledge dissemination openly. The first workshop (Trondheim, 2014) was concerned with steady state operation. The second workshop will focus on transient operations such as load variation and start-stop. In the present work, 2-D particle image velocimetry (PIV) with synchronized pressure measurements performed in the draft tube cone of the Francis-99 test case during load rejection is presented. Pressure sensors were mounted in the vaneless space and draft tube cone to estimate the instantaneous pressure fluctuations while operating the turbine from the best efficiency point (9.8°) to part load (6.7°) with the presence of a rotating vortex rope (RVR). The time-resolved velocity and pressure data are presented in this paper showing the transition in the turbine from one state to another.

1. Introduction

The penetration of the electricity generated from the solar and wind has raised significant concern about the grid stability [1]. The hydropower power plant is used to balance the grid parameters because of the speedy and smooth response to grid network of the hydraulic turbines. Therefore, turbines have to sustain transient phenomena's such as load variation and start-stop. This leads to the unsteady pressure pulsation and development of complex flow in the runner, vaneless space, and draft tube [2- 3]. Reduced scale mode testing and computational fluid dynamics (CFD) are the main tools for design and analysis of turbine. Increased computational capacities and coupling of flow parameters have given more importance to CFD in order to investigate the complexity of the flow in the turbine [4, 5]. The extensive amount of measurements on both prototype and reduced-scale model Francis turbine had been performed to investigate these instability [2, 6-9]. A set of workshops (Francis-99) have been planned to provide an open access of the complete design and data of model Francis turbine during steady and transient operations. The main objective of the workshop was to evaluate the numerical techniques applied to investigate the hydraulic turbines and develop an open platform to the researchers for conducting numerical studies in high head turbines. The first workshop (Trondheim, 2014) was concerned with steady operation [10]. A total of 14 research papers were presented. The second workshop will be a continuation of the first workshop with new steady state operating conditions. There will also be a focus on the simulation of the flow during transient operation such as load variation and start-stop. In order to prepare the second workshop, 2-D particle image velocimetry (PIV) and pressure measurements were performed in the draft tube cone of the Francis-99 test case during load rejection (best efficiency point to part load), load acceptance (best efficiency point to high load), and start-stop. These data are available on the workshop website (https://www.ntnu.edu/nvks/francis-99). In the present work, detailed investigation of load rejection will be presented. The aim of the present study is to investigate the unsteady flow pattern and pressure pulsation inside the draft tube during load rejection. The motivation behind the study is to create a good quality data base in order to understand the consequence of the transient operations and validate future transient simulations of the investigated

model. This may allow with time to develop new guide vanes operating strategy to minimize the dynamic instability in the Francis turbine.

2. Material and Method

2.1. Model test rig

A scale (1:5.1) model of a prototype Francis turbine has been selected for the present investigation. The model turbine is installed at the Water Power Laboratory, Norwegian University of Science and Technology (NTNU), Norway. The prototype turbine (Head =377 m, Power =110 MW, and Runner diameter =1.779 m, Discharge = 31 m^3s^{-1}, Specific speed=0.27) is in operation at Tokke power plant, Norway. A schematic of the test rig is presented in Fig.1. Water from the basement was pumped to the overhead tank which flowed down to the upstream pressure tank connected to the turbine inlet. A uniform level of the water was maintained in the overhead tank. The draft tube was connected to the downstream tank, which was open to the air, and the water was released back to the basement. The model is integrated with 14 stay vanes conjoined inside the spiral casing, 28 guide vanes, a runner with 15 splitters and 15 full length blades, and an elbow-type draft tube. At the inlet pipeline, two pressure transmitters, PTX1 and PTX2 were mounted at 4.87 m and 0.87 m upstream of the turbine inlet, respectively. A magnetic flow meter was used to measure the turbine discharge and a differential pressure transducer was used to acquire the pressure difference across the turbine.

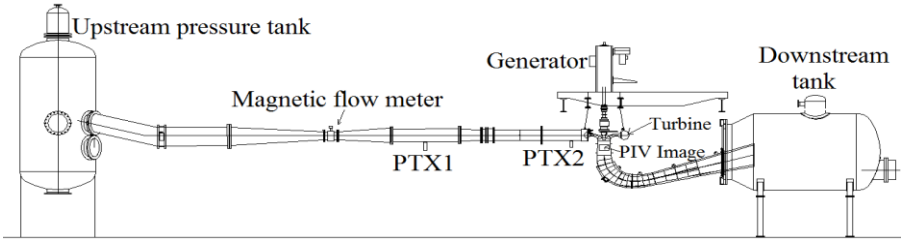

Figure.1 Test rig of the model Francis turbine

2.2. Pressure and velocity measurements , Instrumentation, and Calibration

The instrumentation, calibration, measurements procedure, and data analysis were carried out according to the guidelines available in IEC 60041[11], IEC 60193[12], and ASME PTC 18 [13]. The pressure measurements were recorded using a National Instruments (NI) Compact Reconfigurable Input /Output (cRIO) Model 9074 with a 24 bit analog to digital converter (ADC). The data were sampled at 5 kHz for each channel. The operating and flow parameters such as discharge, turbine inlet and differential pressure, atmospheric pressure, the angular speed of the runner, shaft torque to the generator, bearing friction torque, turbine axial force, and guide vanes angular position were acquired through the same acquisition system. In addition to the base instrumentation of the test rig, six pressure sensors (Kistler-701A, 0-25 bar) were mounted in the draft tube cone and two pressure sensors (Kulite-Druck PTX 1830, 0-10bar) were mounted in the vaneless space, one near the beginning of the spiral casing and one near the end as shown in Fig. 2 and Table 1. The estimated uncertainties were below 0.01%, for the vaneless space sensors (VL1 and VL2), and draft tube sensors. The estimated uncertainties were below 0.02% for the inlet pipe transducer (PTX1 and PTX2). The total estimated uncertainty was ± 0.15% for the hydraulic efficiency under the steady-state operating condition of BEP.

PIV measurements have been performed in the draft tube with a 2-D PIV system (TSI). The draft tube cone is made of transparent Plexiglas to allow optical access to the flow domain. The pulsed light sheet with a thickness of ~3 mm, was generated by two Nd: YAG PIV laser (maximum frequency=50 Hz) with dual cavity performing 100 mJ by the pulse. The wavelength was 532 nm. The laser was placed on a hydraulic table, in order to provide the vertical movement with minimal horizontal and lateral shift. The lightning field was visualized by a low noise digital charge coupled device (CCD) camera (VC-4MC-M180) of 2048 x 2048 pixel resolution, with a succession of paired images at 300-400 µs. The

camera resolution is 2032 x 2048 pixels for a 276.0 x 278.0 mm^2 spatial domain. The camera was placed on a lightweight traverse table (Dantec), in order to provide a reliable and repeatable camera movement. Seeding particles (TSI, polyamide 12) were used: particle density of 1.016 g/cc, refractive index 1.52 and mean diameter of 55 µm. To minimize the optical distortion, an index matching box (refractive index 1.52) made of glass filled with water, was used for the calibrations and measurements to decrease the light aberration during the PIV measurements. The ex-situ calibration was performed in the draft tube due to practical limitations associated with the in-situ calibrations. A specially designed 2-D target plate with dots having a diameter of 2 mm and spaced every 20 mm was placed inside the draft tube for calibration. During the calibration, the camera is at the same position as during the measurements. A sensitivity analysis test with different sampling rate was performed. It was found that at an acquisition frequency of 40 Hz, the light intensity inside the cone was enough for capturing clear images with CCD camera. 2400 paired images were captured for 60 s at the measurement section.

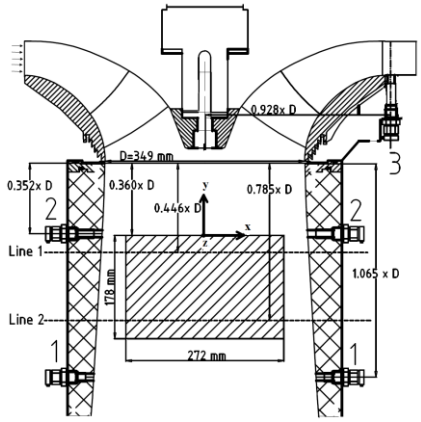

Figure 2 (a). Drawing of the model Francis turbine from side

Table1. Position of pressure sensors

Senso	Placemen	Type
DT1	1A	Kistle
DT2	1B	Kistle
DT3	1C	Kistle
DT4	1D	Kistle
DT5	2B	Kistle
DT6	2D	Kistle
VL1	3E	Kulite
VL2	3F	Kulite

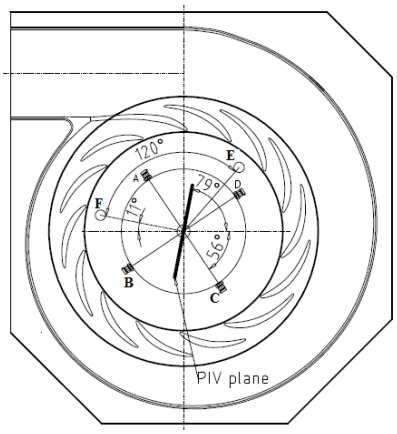

Figure 2(b). Drawing of the model Francis turbine from top

Figure 2. Sensor placement as seen from above Fig. 2(a) from side and Fig. 2(b) from the top. Note that the vaneless sensor taps are 120 degrees apart. All dimensions are in mm. The sensor denomination and their placement are shown in Table 1.

2.3. Measurement program

Both steady-state and transient measurements were performed on the model Francis turbine. The operating conditions were inspired by the operating conditions presented in Francis 99 workshop-I, but with some changes. Since the aim was to perform realistic transient measurements, therefore, the new operating points have the same runner revolutions per minute (RPM) at all operating conditions to achieve the realistic condition as of prototype. The maximum hydraulic efficiency of 92.4 % was found under the steady state condition at α = 9.8°, n_{ED} = 0.18, and q_{ED} = 0.15, marked as best efficiency point (BEP). Additionally, the part load (PL) operating condition has been changed in order to obtain a clear rotating vortex rope (RVR) pulsation in the draft tube. All the measurements were performed in an open loop configuration to get realistic conditions without significant variation of the effective head available to the turbine inlet similar to prototype. The specification of steady-state operating points is presented in Table 2.

Table 2. Operating points

Operating Point	Guide-vane angle (°)	Head (m)	Flow rate (m^3/s)	Hydraulic efficiency (-)
PL	6.7	11.87	0.140	0.90
BEP	9.8	11.94	0.200	0.93

The transient measurement was carried for load rejection by changing the angular position of the guide vanes from 9.8° (BEP) to 6.7° (PL). The maximum angular movement of the guide vanes is 14° (Full Load). Guide vanes are always operating against the acting pressure or hydrodynamic forces. Hence, there may be some difference between the angular position recorded and the actual position of about ±0.044°. The angular position of 6.7° (48%) is the lowest guide vanes angle for the load variation and 14° (100%) is the maximum opening (PM ≈ 30 kW) for the head of 12.5 m used in this study. The generator was operated at n_{ED} = 0.18 during the transient measurements, where flow rate and output power were managed by operating the guide vanes.

2.4. Data analysis for synchronized pressure and velocity measurements

There was a variable time delay for the PIV between receiving a trigger signal, and starting acquisition. In order to determine this time delay, a small light-emitting diode (LED) was placed on the edge of the PIV image frame, and the powering signal for this LED was recorded on the cRIO. The first image with LED-off was recorded manually in all the PIV measurements. A Matlab function was created in order to calculate the time delay between pressure and PIV measurements. The variation of the time delay was the order of seconds, verifying the need for the LED as a synchronization mechanism. Later, the LED was masked out in the processing of the images. The guide vanes movement was operated by a computer-controlled relay, taking both the guide vanes angle and the runner positions from transistor – transistor logic (TTL) as inputs. This ensured that the guide vanes movement began at the same runner position for all the transient repetitions. The commercial PIV software, INSIGHT 4G, from TSI was used for image processing and PIV data analysis. Cross-correlation scheme with smaller (32x32 pixels) spots with two refinement steps and 50 % overlap between the adjacent windows was applied on the acquired data after performing the 2-D calibration. A masking was applied in the processing to remove the unilluminated portion of the image from the processing step. Therefore, 272 x 178 mm^2 area was processed for obtaining the velocity vector field in the draft tube cone. Spectral analysis of the pressure and velocity data were performed to find out the dominant frequencies of the flow and their physical sources. The spectral analysis was performed with Welch's method and applying the Hanning window on the fluctuating part (see Eq.1) of the pressure and velocity data after applying the calibration results to the raw signals.

$$\hat{S}(t) = S(t) - \bar{S} \tag{1}$$

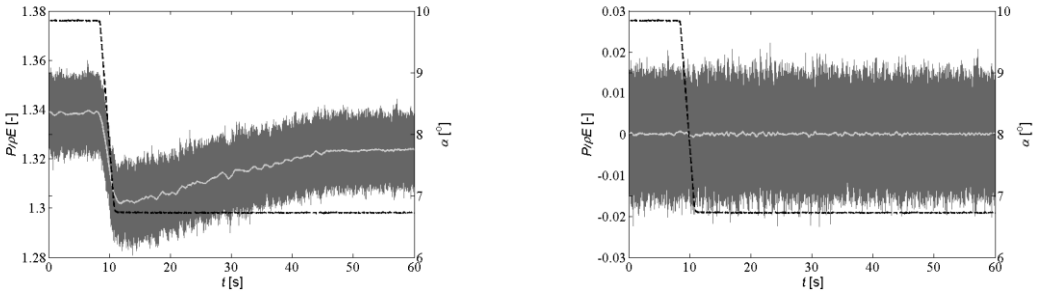

(a) VL1 **(b)** VL1 fluctuating part

Figure 3 (a). Raw and mean pressure signal from the sensor mounted in the vaneless space (VL1) during load rejection from BEP to PL, **3(b).** The fluctuating part of the vaneless sensor (VL1) signal during load rejection from BEP to PL (grey lines: instantaneous pressure , white line : smoothed pressure signal, black dashed line : guide vane angle).

The smoothing of the transient data was carried out using Savitzky-golay filter in Matlab [2]. Subtraction of the smoothed signal from the original one gives the fluctuating part of the signal during the transition; it is used for the frequency analysis. A polynomial of order 2 with a frame size of 1 s was selected as the input parameters for the smoothing function. Figure 3 (a) shows the variation in the signal

of the pressure sensor located at vaneless space (VL1) together with the guide vanes angle variation during load rejection from BEP to PL. Figure 3 (b) shows the fluctuating part of the pressure signal after subtraction of the smoothed pressure signal from the original one. The same smoothing process was applied on the head (H), discharge (Q), and generator torque (T_{GEN}), the results are presented in the next section.

3. Results and Discussion

3.1. Repeatability of the measurements

To ensure the repeatability, the transient measurements were performed twenty times. Synchronized pressure and velocity measurements were performed for all the transient repetitions. In this section, a statistical analysis for discharge (Q), head (H), generator torque (T_{GEN}), and guide vane angle (α) are performed and discussed for all the repetitions during load rejections to estimate the uncertainties involved. All the data were normalized between the minimum value 0 (0%), and the maximum value 1 (or 100%) taking the uniform length of the signal using Eq.2.

$$X[-] = \frac{X - X_{Min}}{X_{\max} - X_{Min}} \tag{2}$$

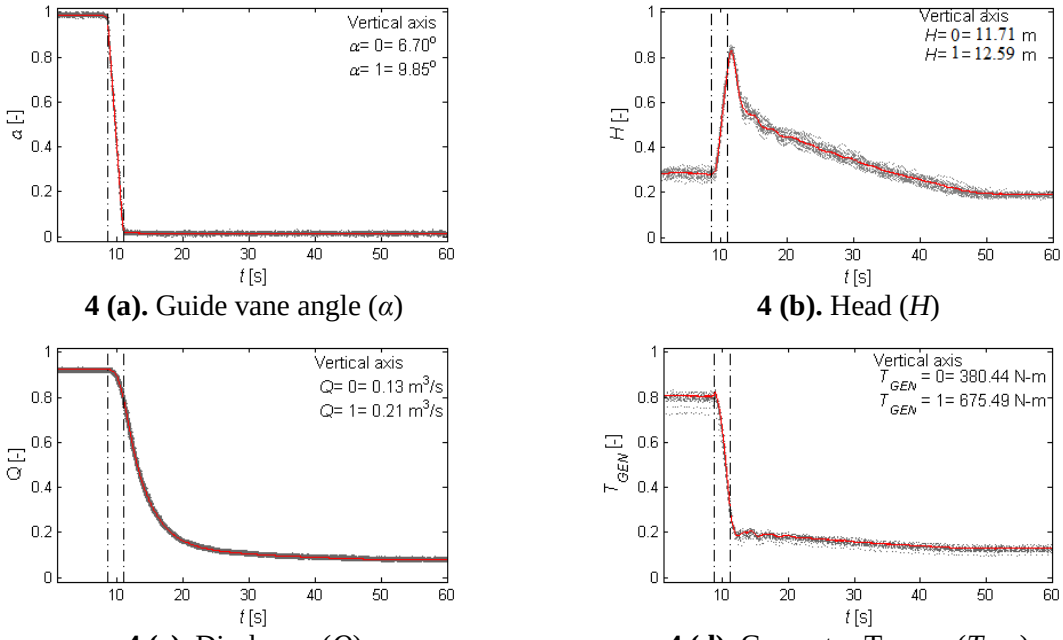

4 (a). Guide vane angle (α) **4 (b).** Head (H)

4 (c). Discharge (Q) **4 (d).** Generator Torque (T_{GEN})

Figure 4. Repetitions for load rejection (BEP to PL), **4 (a)** Guide vane angle (α), **4 (b).** Head (H), **4 (c).** Discharge (Q), and, **4 (d).** Generator Torque (T_{GEN}), grey dot lines: repetitions for load rejection; red line: mean of all the repetitions; black dashed lines: start and end of the transient process.

Figure 4 shows the percentage variation in guide vane angle (α), head (H), discharge (Q), and generator torque (T_{GEN}) for all the repetitions of the load rejection (BEP to PL) operation. The vertical axis (y-axis) represents the variation in the corresponding property. The corresponding steady state values before and after the transient are presented in Fig. 4(a-d). The estimated maximum uncertainties were ±0.08°, ±0.09 m, ±0.003 m^3/s, and ± 4.40 N-m for the guide vanes angle (α), head (H), discharge (Q), and generator torque (T_{GEN}), respectively. The repeatability for the transient operation was found to lie in a certain and acceptable band. Therefore, a single measurement can be trusted and selected for the further investigations. Up to 8.45 s, the turbine was operated at the BEP (9.8°). At 8.45 s, the movement of guide vanes is started and hit at PL (6.7°) operating condition at t=10.90 s (Fig 4). The

torque variation is almost following the guide vanes movement. The flow rate is changing decreasing gradually and become stabilize at around t=48 s. The head is determined by measuring the differential pressure across the turbine and is the most affected parameter due to the development of high-peak pressure pulsations during guide vanes closure.

3.2. Instantaneous high frequency variation in the vaneless space and draft tube

The fluctuating signals from the transient pressure and velocity data were used for spectral analysis. Spectrograms are used to present the transient spectral analysis. The function uses the Goertzel algorithm to analyze the data. The window size of 4.09 s with 95% overlap was selected after a sensitivity analysis on the pressure. Similarly, the spectral analysis of the velocity data was presented after extracting the fluctuating velocity along two points on the PIV plane. The coordinates in millimeters for the two points are P1 (-87.50,-30, 0) and P2 (87.50, -30, 0) according to axis system shown in Fig. 2 (a). The window size of 2 s with 95% overlap was selected after a sensitivity analysis on the velocity. The frequencies in the figure were normalized using the runner rotational frequency (f_n=5.55 *Hz*).The color bar in the spectrogram shows the power spectral density (PSD) of the frequency analysis in logarithmic scale. The following equation was used for the PSD, presented in the spectrogram:

$$PSD_{log} = 10 \times \log(10 \times PSD) \quad (3)$$

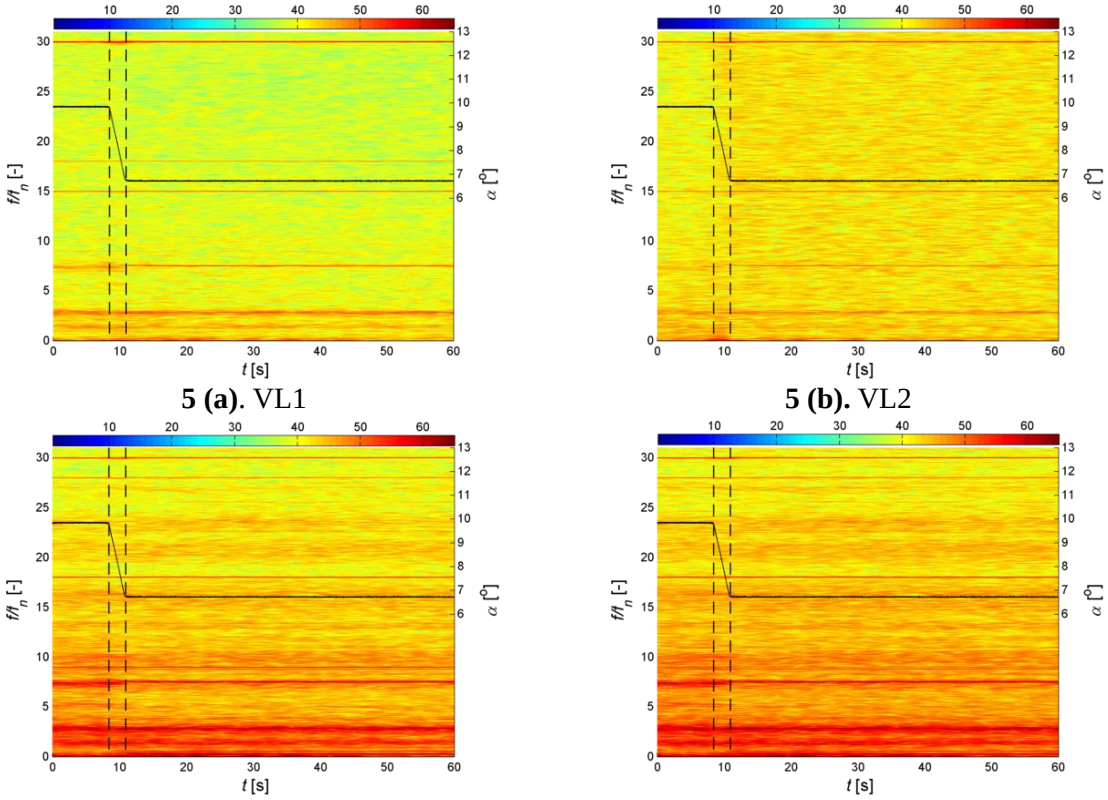

5 (a). VL1 **5 (b).** VL2

5 (c). DT5 **5 (d).** DT6

Figure 5. Spectrogram of the pressure sensor located in the vaneless space and draft tube during load rejection from BEP to PL, **5(a).** VL1, **5(b).** VL2, **5(c).** DT5, and **5(d).** DT6. Black solid line: guide vanes angle (α°); dashed line: start and stop of the guide vanes movement.

The resulting spectrogram of the sensor located at VL1, VL2, DT5, and DT6 during load rejection from BEP to PL are presented in Fig. 5 with a focus on the high frequency region 2-30.f_n. The y axis on the right-side of the spectrogram represents the guide vanes angular movements (α°). For all the sensors,

the blade passing frequency (30.f_n) is present in the pressure signal as expected. The harmonics of the runner frequency (15.f_n) are also present in the vaneless space sensors. Seen in the spectrogram, during transient operation, there is a significant level of fluctuation in the blade passing frequency and its amplitudes. There is a simultaneous change in normalized blade passing frequency from 29.96.f_n to 30.02.f_n. Similar behavior for the blade passing frequency are noticed at all the pressure sensors (VL2, DT5, and DT6) during the transition from BEP to PL but the maximum influence is at the sensor (VL1) near to the spiral casing inlet. The amplitudes of guide vane pass frequency (28.f_n) are also noticed in the draft tube sensors because the frequency is not completely dampened while traveling downstream to the runner.

In the pressure signals, other dominating frequencies are 18.f_n, 7.5.f_n, and 2.9.f_n. The normalized frequency of 18.f_n (100 Hz) was observed in the vaneless space sensor (VL1). This frequency might be attributed to the one–third harmonics of the three phase rectifier and second harmonics of the grid frequency. It is assumed that this frequency will not be available in the system with generator off. The normalized frequency of 7.5.f_n (41.62 Hz) and 2.9.f_n (15.96 Hz) are observed in all pressure sensors. These frequencies might be the standing wave of the system due to the length from the exit of the runner to downstream tank water level (5.6 m) and inlet pipe length to the turbine (14.6 m). Because the sound speed was not experimentally determined, it is assumed to vary between the speed of sound in still water (~1450 m/s) and speed of sound in air (~340 m/s). The amount of air entrapment may vary the speed of sound in the system [14-15]. In the present work, measurements were performed in open loop, increasing the occurrence of entrapped air. Assuming a sound wave velocity of 932 m/s, frequencies are calculated for the upstream and downstream lengths using Eq. 4.

$$f_{sv} = \frac{a}{4L} \tag{4}$$

Where a= sound wave velocity in the system, L = downstream and upstream length

3.3. *Instantaneous low frequency level variation in the draft tube for pressure and velocity signal*
Figures 6-7 show the spectrograms for the low frequencies available in the draft tube for the pressure and velocity data, respectively. The axial (v) and radial (u) velocities data are extracted from the two points P1 and P2 on the PIV plane. The instantaneous recorded pressure and velocity data present the appearance of a low frequency of 0.29.f_n (1.63 Hz) after the transition. This is attributed to the presence of the rotating vortex rope (RVR) in the pressure and velocity data. The harmonics of the RVR frequency are also present in the spectrograms.

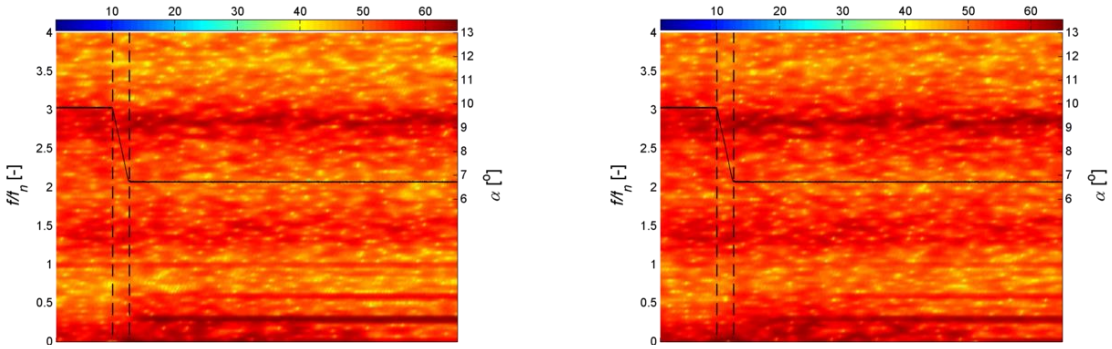

6 (a). DT5 **6 (b).** DT6

Figure 6. Spectrogram of the pressure sensor located in vaneless space and draft tube during load rejection, **6(a).** DT5, **6(b).** DT6, Black solid line: guide vanes angle (α°); dashed line: start and stop of the guide vanes movement

From the spectrograms of the axial and radial velocities for two points P1 and P2 (Fig.7), the time of appearance of the RVR is different for the axial and radial velocities. The velocity spectrograms show

the significant background noise levels (vertical broadband) at some random time intervals with the phenomenal frequencies available in the system. This may be attributed to the low sampling rate (40Hz) of measurement. Usually, noise level is higher from the PIV measurements if the sampling rate is lower than the maximum frequency available in the system [16]. A detailed investigation has been carried out by assuming that there is the existence of a plunging mode of the RVR. These signals are decomposed using the procedure given by Bosioc et al. (2012) [17]. The synchronous (RVR plunging) and asynchronous (RVR rotating) components are determined as below;

$$\frac{(A_1 + A_2)}{2} = \text{Synchronous component}, \quad \frac{(A_1 - A_2)}{2} = \text{Asynchronous component}$$

Where A1 and A2 are the pressure and velocity signals at points P1 and P2, respectively.

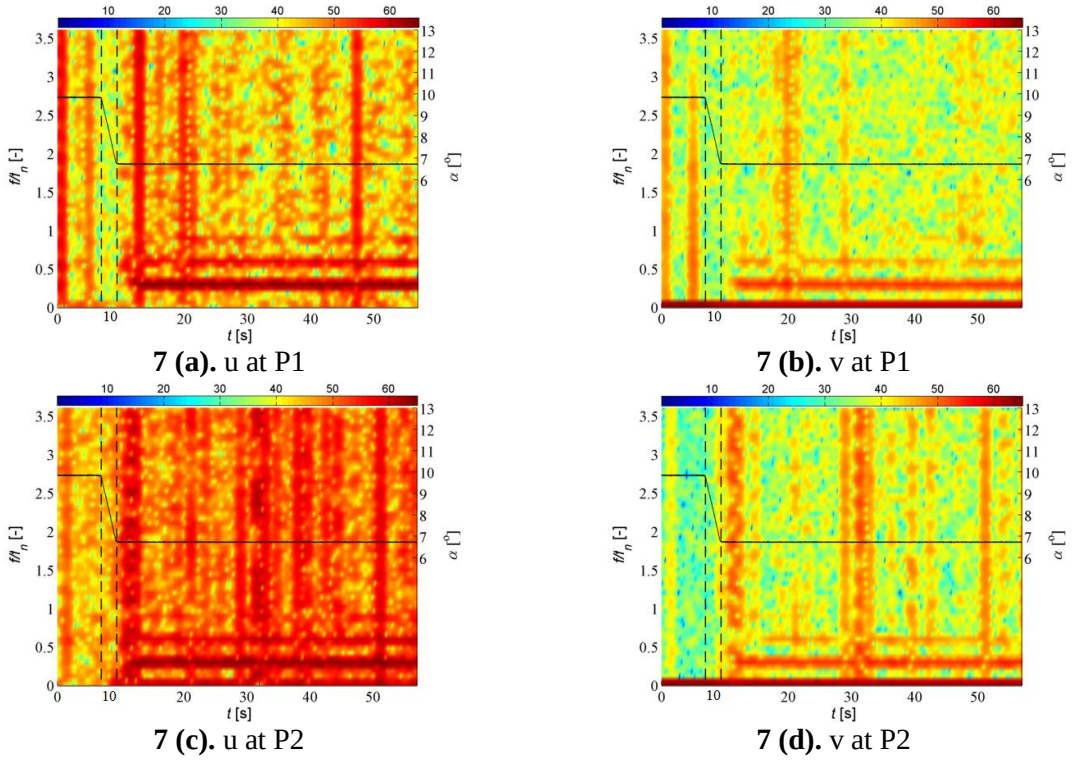

7 (a). u at P1 **7 (b).** v at P1

7 (c). u at P2 **7 (d).** v at P2

Figure 7. Spectrograms of the radial and axial velocities for two points (P1 and P2) data extracted from the PIV vector field, Black solid line: guide vanes angle (α°); dashed line: start and stop of the guide vanes movement

The dimensional amplitudes variation of the RVR for the plunging and rotating modes during load rejection (BEP to PL) are presented in Fig.8. The RVR plunging mode appears 0.8 s before the rotating mode**.** The amplitude of the RVR rotating mode is larger than the plunging mode as shown in Fig. 8 (a) for the draft tube pressure sensors. The amplitudes of the RVR in the plunging mode appear to be stronger at the end of the transient. The same procedure to resolve the RVR rotating and plunging mode is applied to the radial (u) and axial (v) velocities separately for the two points (P1 and P2) which are extracted from the PIV vector field. Fig. 8 (b) and Fig. 8(c) present the time of appearance of the RVR rotating mode and plunging mode in the draft tube for the radial and axial velocities, respectively. In Fig. 8(b) and Fig. 8(c), the amplitude of the plunging mode does not appear in the radial velocity and the amplitude of rotating mode does not appear in the axial velocity for the two radially apart points P1 and P2. Therefore, the radial velocity is only involved in the RVR rotating mode and the axial velocity in the RVR plunging mode.

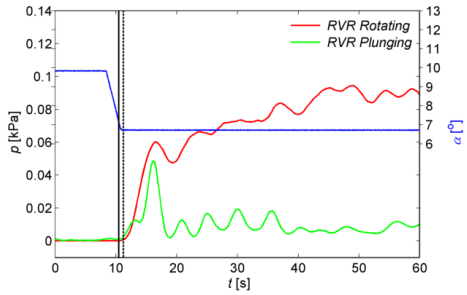

8(a). RVR rotating and plunging mode for draft tube pressure sensors (DT5 and DT6)

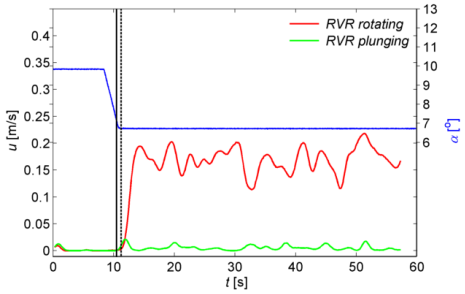

8(b). RVR rotating and plunging mode of the radial velocity assuming point P1 and P2

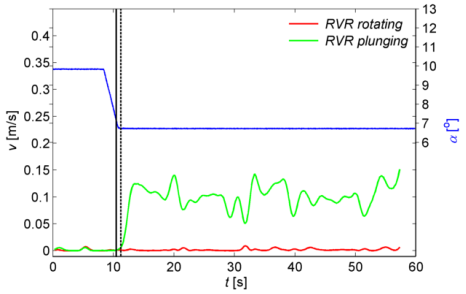

8(c). RVR rotating and plunging mode of the axial velocity assuming point P1 and P2

Figure 8. Time of appearance of RVR rotating and plunging mode in the pressure and velocity data, **8(a).** At DT5 and DT6, **8 (b).** At P1 and P2 for radial velocity, and **8(c).** At P1 and P2 for axial velocity, black solid line: appearance of the plunging mode; black dashed line: appearance of the RVR

Conclusions

Unsteady synchronized pressure and velocity measurements were performed in the high head model Francis turbine during load rejection from BEP to PL. The aim of the study was to investigate the dominating frequencies available and developed in the system before, in between, and after the transition. The results showed the blade passing frequency is available in the complete flow domain of the system as presented by the spectrograms of the vaneless space and draft tube sensors. The significant level of variation in blade passing frequency level was noticed during the transition phase because flow becomes unstable in the runner blade passage due to mismatch of flow angle between the guide vanes outlets and runner inlet. The standing waves frequencies for downstream and upstream length to the runner are presented and discussed with the assumption of sound-wave velocity available in the laboratory. The frequencies are available in a synchronous mode that indicates these frequencies are independent of the runner frequency. The variation in downstream standing wave frequency after transient have noticed due to change in the downstream tank level with discharge to the turbine. The closing of guide vanes during load rejection (BEP to PL) are causing the swirl in the draft tube and formation of RVR. The RVR frequency was further decomposed into two modes, RVR rotating and RVR plunging. It was observed that the RVR plunging appears 0.8 s before the rotating mode. However, the rotating mode was observed with higher amplitudes in comparison to plunging modes. The RVR rotating and plunging modes were further decomposed with the velocity data and it was observed that the axial velocity only contributes to the development of the plunging mode and radial velocity contributes to rotating mode. The transition (BEP to PL) was performed for the time 8.4 s to 10.9 s. The plunging mode appears in the system in between transition phase at 10.5 s, and rotating mode appears after 0.8 s of plunging mode. The time of appearance of RVR rotating and plunging was found same from the pressure and velocity data.

Acknowledgement

Rahul Goyal and Prof. Michel Cervantes are grateful to the Swedish water power center (SVC) for the financial support. The authors would like to thank the Norwegian Hydropower Centre (NVKS) for the financial support. The measurements have been carried out in collaboration between LTU, Sweden (NTNU, Norway) and IIT Roorkee. The author's gratitude also goes to the staff of water power laboratory, NTNU, Norway.

References

[1] Trivedi C, Gandhi B K, and Cervantes M J 2013 *J. of Hydraulic Research* **51 (2)** 121

[2] Trivedi C, Gandhi B K, Cervantes M J and Dahlhaug O G 2014 *J. of Hydraulic Research* **52 (2)** 283

[3] Amiri K, Mulu B, Raisee M and Cervantes M J 2015 *J. of Hydraulic Research* **54 (1)** 56

[4] Keck K and Sick M 2008 *ActaMech* **201** 211

[5] Cervantes M J, Andersson U and Lövgren H M 2010 *IOP Conf. Series: Earth and Environmental Science*, **12(1)**, 012014

[6] Vekve T and Skåre P E 2002 Velocity and pressure measurements in the draft tube on a model Francis turbine *Proc. of the XXI Int. Conf. on Hydraulic Machinery and Systems (Lausanne)*

[7] Vekve T 2004 An experimental investigation of draft tube flow *Ph.D. thesis* (Norway: Norwegian University of Science and Technology)

[8] Korbo E, Dahlhaug O G and Nielsen T K 2008 On board pressure measurement in Francis model Runner *Proc. of the XXIV Int. Conf. on Hydraulic Machinery and Systems (Brazil)*

[9] Korbo E 2010 Measurement of pressure pulsation in Francis turbine *Ph.D. thesis* (Norway: Norwegian University of Science and Technology)

[10] Cervantes M J, Trivedi C, Dahlhaug O G and Nielsen T 2015 *J. of Phys.* **579** 011001

[11] IEC 60041 1991-11 Field acceptance tests to determine the hydraulic performance of hydraulic Turbines, storage pumps and pump-turbines *International Electrotechnical Commission* (*Geneva, Switzerland*)

[12] IEC 60041 1991-11 Hydraulic turbines, storage pumps and pump turbines- model acceptance test *International Electrotechnical Commission* (*Geneva, Switzerland*)

[13] ASME-PTC18 2011 Hydraulic turbines and pump-turbines performance test codes *ASME New York*

[14] Nielsen T 1990 Transient characteristics of high head Francis turbines *Ph.D. thesis* (Norway: Norwegian University of Science and Technology)

[15] Knudsen H 2008 Study of the speed of sound in pipes and pulse reflections for open and closed boundary conditions and non-return valve *Ph.D. thesis* (Norway: Norwegian University of Science and Technology)

[16] Koschatzky V, Boersma B J, Scarano F and Wasterweel J 2011 High speed PIV applied to aerodynamics noise investigation *VIII International symposium on particle image velocimetry-PIV09* (*Melbourne, Victoria, Australia*)

[17] Bosioc A L, Resiga R S, Muntean S and Tanasa C 2012 *J. of Fluids Eng.* **137** 081104-1